Reliability analysis and micromechanics: A coupled approach for composite failure prediction

H. Welemane [a,*], H. Dehmous [b]

[a] Université de Toulouse; INP/ENIT; LGP; 47, avenue d'Azereix, F-65013 Tarbes, France
[b] Université de M'sila, BP 166, 28000 M'sila, Algerie

* Corresponding author. Tel.: +33 5 62 44 29 47; fax: +33 5 62 44 27 08.
E-mail address: Helene.Welemane@enit.fr (H. Welemane).

A B S T R A C T

This work aims at associating two classical approaches for the design of composite materials: first, reliability methods that allow to account for the various uncertainties involved in the composite materials behaviour and lead to a rational estimation of their reliability level; on the other hand, micromechanics that derive macroscopic constitutive laws from micromechanical features. Such approach relies on the introduction of variabilities defined at the microscale and on the investigation of their consequences on the material macroscopic response through an homogenization scheme. Precisely, we propose here a systematic treatment of variability which involves a strong link between micro- and macroscales and provides a more exhaustive analysis of the influence of uncertainties. The paper intends to explain the main steps of such coupling and demonstrate its interests for material engineering, especially for constitutive modelling and composite materials optimization. An application case is developed throughout on the failure of unidirectional carbon fibre-reinforced composites with a comparative analysis between experimental data and simulation results.

Keywords:
Reliability
Micromechanics
Composite materials
Failure

1. Introduction

If mechanical performances of composite materials offer gradually attractive design perspectives for many industrial applications, huge safety margins introduced owing to the important scatter of their properties still appear as a strong limitation for their large development. Recently structural reliability analyses [1,2] have allowed significant progress in the conception phases and for maintenance programs through a more rational estimation of the risk exposure. By considering the parameters of a structure (for instance loads, geometry, materials properties, etc.) as random variables, these methods account for uncertainties arising and provide either a quantitative evaluation of the failure probability for a given application or a range of use to achieve a specified reliability level.

Obviously, the relevance of results obtained by such analyses highly depends on the problem representation retained, and then especially on the mathematical modelling of the materials behaviour. In the case of heterogeneous materials, the macroscopic response results from mechanisms occurring at the microscale within their constituents and at their interfaces, and from the spatial distribution of these constituents. From the definition of a representative volume element of the composite material, classical homogenization techniques offer in such context a rigorous framework to derive its overall behaviour from local informations [3–5].

Accordingly, the association of probabilistic modelling and micromechanics seems to be an interesting and appropriate way to achieve consistent characterizations of composite behaviours [6]. In addition to the description of fluctuations at various scales, such approach can also integrate the microscopic origin of failure and confers a clear physical meaning to material reliability. Most of failure models developed in this sense uses a local failure criteria (on composite constituents and/or on the interfaces) with a statistical distribution of strength parameters (generally of Weibull type) and assumes equal or local load sharing to represent the damage growth. In this case, homogenization techniques enable the estimation of the composite effective behaviour and the derivation of local fields from macroscopic solicitation [7–10].

In keeping with such probabilistic micro–macro approaches, the present work stands out by a more exhaustive treatment of variability. We propose indeed an explicit association of reliability methods and micromechanics that creates a link between micro- and macroscales concerning the effects of uncertainties. The main objectives associated to this approach are:

- to capture a large amount of inherent fluctuations at the microscale (constituents properties, morphological features, etc.) and analyse their consequences on the composite macroscopic reliability; from this, one can deduce the most significant micromechanical parameters and, for example, steps that

need special care in the manufacturing process to enhance the design and optimization of given structural applications;
- more generally, to develop interactions between micromechanics and probabilistic modelling; first, the introduction of statistical data provides enriched identification and validation procedures of micromechanical models; then, reliability indicators can help to quantify their sensitivity to assumptions retained and therefore to improve representations.

Section 2 of this paper will describe the general background of such coupled approach, namely recall the different steps of a classical reliability analysis and precise where micromechanical aspects are introduced. We present in Section 3 the case study of this paper, namely a unidirectional carbon-epoxy composite, and the micromechanical formulation chosen to represent its behaviour is detailed in Section 4. The reliability model and simulation procedure are presented in Section 5. From the comparison between experimental reliability and simulation results, the final discussion of Section 6 will illustrate the aforementioned advantages of the approach, especially the estimation of relative importance of uncertainties introduced or modelling adjustments that can be deduced.

2. General background

Structural reliability analyses allow the performance estimation of systems which exhibit notable fluctuations that cannot be captured by deterministic models. In the present study, we focus on the reliability of a mechanical system component (later referred as the "structure") associated to a heterogeneous material. In view of this, a reliability analysis requires three important steps:

- first, the selection of N input random variables (denoted by vector $X = \{X_i\}_{i=1,..n}$) that describe the various sources of uncertainties arising;
- then, the choice of a failure scenario which is mathematically defined by a limit state function G;
- and finally, the calculation of indicators (such as the mechanical system failure probability P_f) which provide a qualitative and quantitative evaluation of the structure reliability.

Considering the first point, uncertainties affecting composite materials concern both the microscopic level which is relative to the material microstructure (constituents properties, spatial distribution, interfaces characteristics, presence of defaults, etc.) and the macroscopic level (model relevance, composite properties, structure geometry, load, etc.). Most often, they come from the material manufacturing process, results dispersion in experimental characterization (poor testing reproductibility, scale effects, etc.), load variability or simply by the lack of knowledge of some data. In the present approach, the choice of random variables is motivated by two arguments:

- material design and optimization perspectives, so that most of microstructural parameters that can be governed in some way during manufacturing process need to be included;
- availability of experimental results, which can justify probabilistic models associated to random variables (in particular their joint probability function f_X, otherwise marginal density functions $\{f_{X_i}\}_{i=1..N}$, and correlations relations) and provide consequently physical consistent representations.

The second requirement is the definition of the failure scenario defining the limit state beyond which the structure is not considered as reliable. According to the study objectives, such limit state may correspond either to some mechanical strength achievement or to serviceability. From this, one needs to define the performance (or limit state) function G which denotes the boundary in the space of X between the safe domain $\mathcal{D}_s$ (such that $G(X) > 0$) and the failure domain $\mathcal{D}_f$ (such that $G(X) \leq 0$). Important aspects relative to the choice of the failure criterion are as follows:

- expression of G should be motivated by the physical origin of the failure scenario in order to derive a realistic representation of the structure reliability; in the case of heterogenous materials, it may concern either microscopic features (for local failure modes) or macroscopic data (for structural instabilities);
- if G has an implicit definition based on the mechanical response of the structure, the analysis will involve a coupling between reliability methods and a mechanical model (if necessary associated to finite-element simulations);
- finally, practical aspects can influence the decision (especially simulation time), in view of the complexity of the previous coupling or mathematical properties of G.

The calculation of reliability indicators constitutes the last step of a reliability analysis. Considering only time independent case, the probability of failure is given by

$$P_f = Prob(G(X) \leq 0) = \int_{\mathcal{D}_f} f_X(X) \prod_{i=1}^{N} dX_i \tag{1}$$

For most practical problems, it is well known that the formulation of f_X and its integration over the failure region is typically too difficult to be computed directly. Among numerical methods developed to estimate P_f [1,2], approximation methods (FORM/SORM) that rely on simplifications of the failure domain are clearly computationally efficient. Moreover, they provide in addition to P_f a sensitivity analysis that identifies the influence of random parameters (importance and nature [11,12]). Such complementary information is very useful in view of the both objectives of the present work.

It was important to present from the beginning the main guidelines of the reliability analysis and in which way informations relative to the microscale should be introduced. Indeed, all choices and assumptions retained in what follows (on random variables, mechanical modelling, failure scenario, numerical implementation) will be governed by before-mentioned objectives and recommendations.

3. Material description and experimental data

The engineering case investigated in this paper concerns composite stay cables used for the first time in France in 2002 by the Freyssinet International Company for the execution of the Laroin pedestrian footbridge ([13], Fig. 1). Each stay cable of this structure is composed of two or three strands of seven carbon-epoxy cylindrical rods (Fig. 2).

This work deals with the reliability assessment of these composite rods that correspond to the cables elementary structure. Manufactured by the SOFICAR company (SOciété des FIbres de CARbone, Company of Carbon Fibre, located in Abidos, France), these pultruded unidirectional composite rods are composed of aligned TORAYCA high-strength carbon fibres T700SC-12K, embedded in an epoxy resin Eponal 401 manufactured by BOSTIK FINDLEY (mean fibre volume fraction of 67%) (Fig. 3). For the validation of the rods model, one needs in what follows to investigate the behaviour of another pultruded products of SOFICAR, namely unidirectional carbon-epoxy composite laminates

Fig. 1. The Laroin footbridge (France, Pyrénées Atlantiques).

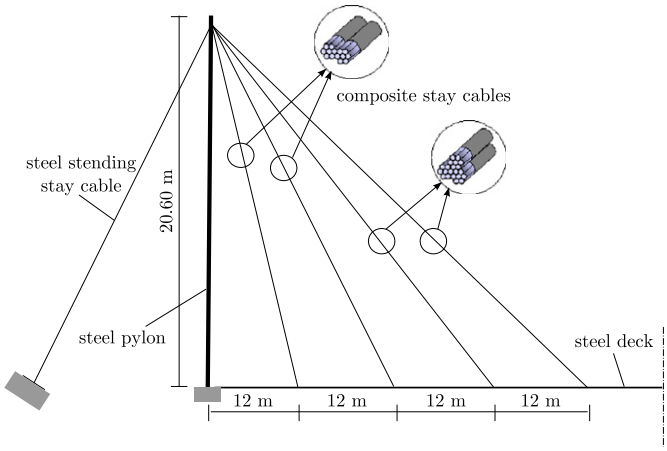

Fig. 2. Structure of the footbridge.

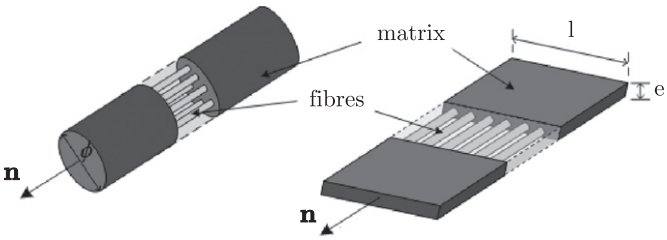

Fig. 3. Composites rods and laminates.

with rectangular section, designed for bridge concrete reinforcement. These laminates are composed of aligned TORAYCA high-strength carbon fibres T800H-2*12K, embedded in the same epoxy resin as rods (mean fibre volume fraction of 62.8%) (Fig. 3).

From the mechanical point of view, fibres exhibit transversally isotropic (around axis given by unit vector $\mathbf{n}$) brittle behaviour and epoxy resin is isotropic viscoelastic [14,15]. Experimental data on components that concern elastic properties and failure values measured under uniaxial tension tests have been provided by manufacturers (Tables 1 and 2). Note that measures on fibres correspond to axial characterizations (along $\mathbf{n}$) and have been obtained on 200 mm length impregnated fibres.

Concerning composite products, SOFICAR have investigated their macroscopic features for quality control, precisely their dimensions (rods diameter $\phi = 6 \pm 0.1$ mm; width $l = 50 \pm 0.3$ mm and thickness $e = 1.2 \pm 0.05$ mm of plates) and their mechanical

Table 1
Mechanical properties of TORAYCA fibres (mean values, source: TORAY).

Fibres	Young modulus, $E_f(\mathbf{n})$ (MPa)	Yield stress, $\sigma_f^F(\mathbf{n})$ (MPa)	Yield strain, $\varepsilon_f^F(\mathbf{n})$ (%)
T700SC-12K	230 000	4870	2.1
T800H-2*12K	294 710	5541	1.88

Table 2
Mechanical properties of Eponal 401 resin (source: BOSTIK).

Young modulus, E_r (MPa)	Yield stress, σ_r^F (MPa)	Yield strain, ε_r^F (%)
2800 ± 125	63.8 ± 4.1	2.4 ± 0.3

performances in the axial direction in view of their own further applications:

- the tensile strength $R^T(\mathbf{n})$ of rods (bridge stay cables), through $N = 158$ tests,
- the elastic modulus $E(\mathbf{n})$ of plates (concrete reinforcement), through $N = 74$ tests [16].

Cumulative frequencies F_i for each of these measures represent the raw experimental data given in Figs. 6, 7 and 11 for $R^T(\mathbf{n})$ and Figs. 9 and 10 for $E(\mathbf{n})$. It should be noted that all the experimental tests have been realized with 200 mm usable length composite samples and on the same test bench INSTRON 4485. An investigation of the precision of the experimental procedure by SOFICAR through a comparative analysis with normalized data (elastic modulus and tensile strength) has shown a minorating error of their device of maximum 3%: raw data of SOFICAR represent indeed among 97% and 100% of normalized values.

4. Micromechanical modelling

Classical homogenization techniques, and especially estimation methods, constitute a very appropriate framework to establish the mechanical model of the material since they provide (see [3–5] for a review):

- on one hand, the overall behaviour of heterogenous materials from microstructural features and components behaviours; this allows the introduction of random parameters relative to the local scale and also the model validation through macroscopic properties;
- on the other hand, an estimation of strain or stress local fields during the load, which is useful for the definition of the failure scenario.

The representative volume element (RVE) V corresponds here to the sample used for quality control itself, that is the 200 mm length cylindrical rod or rectangular laminate, that can be considered as statistically homogeneous in regard to the fibres dimension (cylindrical filaments of 8 μm diameter). The material exhibits a 'matrix-inclusion' morphology since fibres have the same shape, orientation and mechanical behaviour. According to the manufacturing process (pultrusion), fibres are randomly spatially distributed within the RVE, the matrix is continuous and interfaces can be considered as perfect. Concerning the solicitation, small perturbations, rate independent and isothermal conditions are considered. Due to the predominance of fibres properties and the kind of solicitation applied to the composite (longitudinal tension), the viscous aspect

of the matrix can be neglected and all components are assumed to be linear elastic.

The choice of the appropriate homogenization scheme relies on various parameters, such as the geometry of the heterogenous material, the mechanical contrast between phases or the particle volume fraction [17]. Even if some limitations can appear for high carbon fibres volume fraction, we have chosen to use the well-known Mori–Tanaka estimate [18] for following reasons: it represents the overall material anisotropy induced by oriented reinforced fibres (through the Eshelby tensor), allows the introduction of various microstructural features (shape of constituents, etc.) and accounts in some way for the interactions between constituents [19]; moreover, in comparison to iterative schemes (self-consistent, differential, etc.), such formulation provides explicit expressions of the overall elasticity and local fields, which greatly simplify the coupling with reliability analysis.

Usual intrinsic notations are employed throughout. All tensors used in this study are defined on the Euclidean vectorial space $\mathbb{R}^3$ for which the set of vectors $(\mathbf{e}_1,\mathbf{e}_2,\mathbf{e}_3)$ constitutes an orthonormal basis. Especially, T^k represents the vectorial space of tensors of order k ($k\in\mathbb{N}$). In order to make clear expressions in the paper, the inner products are labelled as follows: $a\cdot b$, $\forall(a,b)\in(T^1=\mathbb{R}^3)^2$; $a{:}b$, $\forall(a,b)\in(T^2)^2$; $a{::}b$, $\forall(a,b)\in(T^4)^2$. Additionally, the tensor products of two second-order tensors a and b are defined by

$$\begin{cases}[a\otimes b]:x=(b:x)a, & [a\underline{\otimes}b]:x=a\cdot x\cdot b^T\\ [a\overline{\otimes}b]:x=a\cdot x^T\cdot b^T, & a\underline{\overline{\otimes}}b=\frac{1}{2}(a\underline{\otimes}b+a\overline{\otimes}b)\end{cases} \tag{2}$$

for any tensor $x\in T^2$. In particular, the term $a^{\otimes l}=a\otimes a..\otimes a$ represents the lth tensor product of a tensor a ($l\in\mathbb{N}$).

4.1. General formulation

Let denote by $\boldsymbol{\sigma}$ and $\boldsymbol{\varepsilon}$ (respectively $\boldsymbol{\Sigma}$ and $\mathbf{E}$) the stress and strain local (resp. macroscopic) fields. In the Mori–Tanaka formulation, the matrix is considered as the reference medium and is subjected to its own stress. The composite compliance tensor $\mathbb{S}_{MT}^{hom}$ such that $\mathbf{E}=\mathbb{S}_{MT}^{hom}:\boldsymbol{\Sigma}$ is then given by

$$\mathbb{S}_{MT}^{hom}=\mathbb{S}_{(m)}+f_i(\mathbb{S}_{(i)}-\mathbb{S}_{(m)}):\langle\mathbb{B}\rangle_{(i)}^{MT} \tag{3}$$

where $\mathbb{S}_{(k)}$ denotes the compliance tensor respectively of the matrix ($k=m$) and of the inclusion ($k=i$) and $f_i=|V_i|/|V|$ the inclusion volume fraction (V_i the inclusion volume within RVE). The stress concentration tensor, $\langle\mathbb{B}\rangle_{(i)}^{MT}$, that provides the average stress over the inclusion phase

$$\langle\sigma\rangle_{(i)}=\frac{1}{|V_i|}\int_{V_i}\sigma\,dV=\langle\mathbb{B}\rangle_{(i)}^{MT}:\boldsymbol{\Sigma} \tag{4}$$

takes the following expression ($\mathbf{I}$ the second-order unit tensor):

$$\langle\mathbb{B}\rangle_{(i)}^{MT}=\langle\mathbb{B}\rangle_{(i)}^{dil}:[(1-f_i)\mathbf{I}\,\underline{\overline{\otimes}}\,\mathbf{I}+f_i\langle\mathbb{B}\rangle_{(i)}^{dil}]^{-1} \tag{5}$$

where the stress concentration tensor of the dilute scheme $\langle\mathbb{B}\rangle_{(i)}^{dil}$ depends on the Eshelby tensor $\mathbb{S}_{(m)}^{E}$ of the inhomogeneity within the matrix ([20,21]; see expressions in Appendix A):

$$\langle\mathbb{B}\rangle_{(i)}^{dil}=\mathbb{S}_{(i)}^{-1}:[\mathbf{I}\underline{\overline{\otimes}}\mathbf{I}+\mathbb{S}_{(m)}^{E}:\mathbb{S}_{(m)}:(\mathbb{S}_{(i)}^{-1}-\mathbb{S}_{(m)}^{-1})]^{-1} \tag{6}$$

4.2. Base model

As a starting point, the mechanical model is built upon simple assumptions concerning the components nature, shape and behaviour:

1. the porosity within the resin is negligible; the matrix medium corresponds then directly to the epoxy resin material ($\mathbb{S}_{(m)}=\mathbb{S}_{(r)}$ and $\mathbb{S}_{(m)}^{E}=\mathbb{S}_{(r)}^{E}$) and the fibres represent the inclusion phase ($\mathbb{S}_{(i)}=\mathbb{S}_{(f)}$ and $f_i{=}f_f$ the fibres volume fraction);
2. the fibres phase is modelled as a cylindrical inclusion of axis $\mathbf{n}$ with circular section, the Eshelby tensor is then given by Eq. (A.4);
3. fibres are assumed to be isotropic with mechanical properties corresponding to their axial features, namely the Young modulus E_f and the Poisson ratio ν_f are taken:

$$\begin{cases}E_f=E_f(\mathbf{n})\\ \nu_f=\nu_f(\mathbf{n},\mathbf{t})\end{cases} \tag{7}$$

whatever the unit vector $\mathbf{t}$ orthogonal to $\mathbf{n}$. According to assumptions 1 and 3, the compliance tensors of components has the form:

$$\mathbb{S}_{(j)}=\frac{1+\nu_j}{E_j}\mathbf{I}\underline{\overline{\otimes}}\mathbf{I}-\frac{\nu_j}{E_j}\mathbf{I}\otimes\mathbf{I} \tag{8}$$

with ($j{=}r$) for the resin and ($j{=}f$) for the fibres.

From this, relevant calculations give rise to the following expression of the stress concentration tensor on the fibres phase expressed within the basis $\{\mathbb{F}_l\}_{l=1,6}$ defined in Appendix A (Eq. (A.1)):

$$\langle\mathbb{B}\rangle_{(i)}^{MT}=\langle\mathbb{B}\rangle_{(f)}^{MT}=\sum_{l=1}^{6}b_l\mathbb{F}_l \tag{9}$$

with

$$b_1=\frac{2E_f}{D}[(1-f_f)(1-\nu_r\nu_f)E_r+f_f(1-\nu_r^2)E_f]$$

$$b_2=\frac{E_f}{D}[(1-f_f)(1-\nu_f-2\nu_r\nu_f)E_r+[1+\nu_r+f_f(1-\nu_r-2\nu_r^2)]E_f]$$

$$b_3=\frac{4(1-\nu_r^2)E_f}{(1-f_f)(1+\nu_f)E_r+(3-4\nu_r+f_f)(1+\nu_r)E_f}$$

$$b_4=\frac{2(1-\nu_r)E_f}{(1-f_f)(1+\nu_f)E_r+(1+f_f)(1+\nu_r)E_f}$$

$$b_5=-\frac{(1-f_f)E_f}{D}[(\nu_r-\nu_r\nu_f-2\nu_f)E_r+\nu_r(1+\nu_r)E_f]$$

$$b_6=\frac{(1-f_f)(\nu_f-\nu_r)E_rE_f}{D} \tag{10}$$

and

$$D=(1-f_f)^2(1-\nu_f-2\nu_f^2)E_r^2+f_f[1+f_f(1-2\nu_r)](1+\nu_r)E_f^2+(1-f_f)[1+\nu_r+f_f(2-\nu_r-\nu_f-4\nu_r\nu_f)]E_rE_f \tag{11}$$

4.3. Model uncertainties

The assumptions retained for the base model have been considered mainly in view of the lack of exhaustive experimental data concerning some points. As a result, some aspects that can affect the composite mechanical behaviour are not taken into account, which introduces modelling uncertainties on the representation obtained. In order to investigate the influence of such simplifications, we propose to reconsider separately each of the previous assumptions.

4.3.1. Matrix porosity

If the resin formulation and the manufacturing process are not fully optimized, the composite matrix may exhibit some notable rate of porosity. Compared to the base model, such phenomena

will affect the matrix properties which should be considered in its turn as a heterogenous material (Fig. 4).

Such problem is carried out with two successive homogenization procedures (the different scales being assumed to be well separated):

- the first one is performed at the scale of the porous resin (RVE), which is considered as a two-phase material with resin as the matrix ($\mathbb{S}_{(m)}=\mathbb{S}_{(r)}$ and $\mathbb{S}^E_{(m)}=\mathbb{S}^E_{(r)}$) and pores as spherical inclusion phase ($\mathbb{S}_{(i)}=\mathbb{S}_{(p)}=\mathbb{O}$ and $f_i=f_p$ the porosity); combining the expression (A.3) of the Eshelby tensor leads finally to the resulting isotropic behaviour of the porous resin with a compliance tensor $\mathbb{S}_{(j)}=\mathbb{S}_{(pr)}$ of the form (8) with effective Young modulus E_{pr} and Poisson ratio ν_{pr} such that

$$\begin{cases} E_{pr}=\dfrac{2(1-f_p)(7-5\nu_r)E_r}{2(7-5\nu_r)+f_p(1+\nu_r)(13-15\nu_r)} \\ \nu_{pr}=\dfrac{2\nu_r(7-5\nu_r)+f_p(3-2\nu_r-5\nu_r^2)}{2(7-5\nu_r)+f_p(1+\nu_r)(13-15\nu_r)} \end{cases} \tag{12}$$

- the second one is done at the composite scale (RVE), which is considered as a two-phase material with porous resin as the matrix ($\mathbb{S}_{(m)}=\mathbb{S}_{(pr)}$ and $\mathbb{S}^E_{(m)}=\mathbb{S}^E_{(pr)}$) and fibres as the cylindrical inclusion phase with spherical section ($\mathbb{S}_{(i)}=\mathbb{S}_{(f)}$ and $f_i=f_f$ the fibres volume fraction); this step is clearly identical to the base model homogenization and can be achieved substituting the following properties in the result (9):

$$\begin{cases} E_r \to E_{pr} \\ \nu_r \to \nu_{pr} \end{cases} \tag{13}$$

4.3.2. Fibres shape

The question of the circular shape of the cylindrical fibres phase is investigated here. Indeed, some steps of the pultrusion process may induce some compression in the cross-section of manufactured composites (die, pulling), leading to a more complex shape for the fibres within the final product. In order to access the impact of such feature, we consider an elliptical section for the cylindrical inclusion.

Let denote by the unit orthogonal vectors $\mathbf{t}$ and $\mathbf{k}$ the ellipse principal axes such that $(\mathbf{n},\mathbf{t},\mathbf{k})$ represents an orthonormal basis of $\mathbb{R}^3$, (a_t,a_k) the minor and major semi-axes (Fig. 5) and $\lambda=a_t/a_k\in[0,1]$ its aspect ratio ($\lambda=1$ corresponds to the circular section).

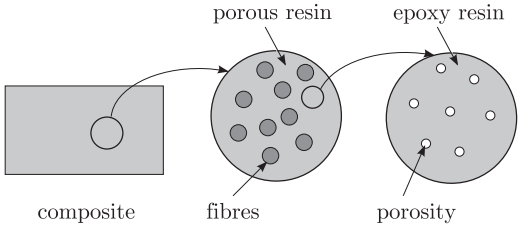

Fig. 4. Scale separation.

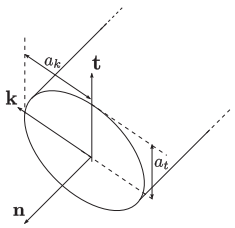

Fig. 5. Cylindrical inclusion with elliptical section.

In that case, the expression (A.5) of the Eshelby tensor leads to a stress concentration tensor on the fibres phase on the form:

$$\langle\mathbb{B}\rangle^{MT}_{(i)}=\langle\mathbb{B}\rangle^{MT}_{(f)}=\sum_{l=1}^{12}b'_l\mathbb{G}_l \tag{14}$$

with the basis $\{\mathbb{G}_l\}_{l=1,12}$ defined in Appendix A (Eq. (A.2)). Since the inversion of fourth-order tensors expressed in such a basis cannot be done explicitly, the components $\{b'_l\}_{l=1,12}$ are obtained through numerical computations.

4.3.3. Fibres behaviour

High-performance carbon fibres are produced from drawn polyacrylonitrile (APN) fibres by a process of controlled pyrolysis followed by a high-temperature heat treatment. The resulting fibres are strongly anisotropic, namely transversally isotropic around their axis $\mathbf{n}$, because of the preferential molecular orientation of the drawn precursor. Written in the orthonormal basis $(\mathbf{n},\mathbf{t},\mathbf{k})$ of $\mathbb{R}^3$, their elastic behaviour is consequently entirely described by five parameters:

$$\begin{aligned}\mathbb{S}_{(f)}=&\frac{1-\nu_f(\mathbf{t},\mathbf{k})}{E_f(\mathbf{t})}\mathbb{F}_1+\frac{1}{E_f(\mathbf{n})}\mathbb{F}_2+\frac{1+\nu_f(\mathbf{t},\mathbf{k})}{E_f(\mathbf{t})}\mathbb{F}_3\\&+\frac{1}{2\mu_f(\mathbf{n},\mathbf{t})}\mathbb{F}_4-\frac{\nu_f(\mathbf{n},\mathbf{t})}{E_f(\mathbf{n})}(\mathbb{F}_5+\mathbb{F}_6)\end{aligned} \tag{15}$$

where $E_f(\mathbf{n})$ and $E_f(\mathbf{t})$ $(\forall\mathbf{t})$ are the Young moduli related respectively to the axial and transverse directions, $\nu_f(\mathbf{n},\mathbf{t})$ $(\forall\mathbf{t})$ and $\nu_f(\mathbf{t},\mathbf{k})$ $(\forall(\mathbf{t},\mathbf{k}))$ are the Poisson ratios related respectively to the axial and transverse planes, and $\mu_f(\mathbf{n},\mathbf{t})$ $(\forall\mathbf{t})$ is the shear modulus related to the axial planes. Without any specific experimental characterization, we propose to work here with a simplified type of anisotropy:

- Poisson ratios and shear modulus are kept equal to their values in the base model (isotropic behaviour), that is:

$$\begin{cases} \nu_f(\mathbf{n},\mathbf{t})=\nu_f(\mathbf{t},\mathbf{k})=\nu_f \\ \mu_f(\mathbf{n},\mathbf{t})=\dfrac{E_f(\mathbf{n})}{2(1+\nu_f(\mathbf{n},\mathbf{t}))}=\dfrac{E_f(\mathbf{n})}{2(1+\nu_f)} \end{cases} \tag{16}$$

- the contrast between axial and transverse Young moduli is described through a scalar parameter $\Theta\in[0,1]$ such that

$$E_f(\mathbf{t})=\Theta E_f(\mathbf{n}) \tag{17}$$

Under these assumptions, one obtains the following expression for the stress concentration tensor:

$$\langle\mathbb{B}\rangle^{MT}_{(i)}=\langle\mathbb{B}\rangle^{MT}_{(f)}=\sum_{l=1}^{6}b''_l\mathbb{F}_l \tag{18}$$

with

$$\begin{cases} b''_1=\dfrac{2\Theta E_f(\mathbf{n})}{D_\Theta}[(1-f_f)(1-\nu_r\nu_f)E_r+f_f(1-\nu_r^2)E_f(\mathbf{n})] \\ b''_2=\dfrac{E_f(\mathbf{n})}{D_\Theta}[(1-f_f)(1-\nu_f-2\nu_r\nu_f\Theta)E_r+\left[1+\nu_r+f_f(1-\nu_r-2\nu_r^2)\right]\Theta E_f(\mathbf{n})] \\ b''_3=\dfrac{4(1-\nu_r^2)\Theta E_f(\mathbf{n})}{(1-f_f)(1+\nu_f)E_r+(3-4\nu_r+f_f)(1+\nu_r)\Theta E_f(\mathbf{n})} \\ b''_4=\dfrac{2(1+\nu_r)E_f(\mathbf{n})}{(1-f_f)(1+\nu_f)E_r+(1+f_f)(1+\nu_r)E_f(\mathbf{n})} \\ b''_5=-\dfrac{(1-f_f)E_f(\mathbf{n})}{D_\Theta}[(\nu_r-\nu_r\nu_f-2\nu_f\Theta)E_r+\nu_r(1+\nu_r)\Theta E_f(\mathbf{n})] \\ b''_6=\dfrac{(1-f_f)(\nu_f-\nu_r)\Theta E_rE_f(\mathbf{n})}{D_\Theta} \end{cases} \tag{19}$$

and

$$\begin{aligned}D_\Theta=&(1-f_f)^2(1-\nu_f-2\nu_f^2\Theta)E_r^2+f_f[1+f_f(1-2\nu_r)](1+\nu_r)\Theta E_f^2(\mathbf{n})\\&+(1-f_f)\begin{bmatrix}\Theta+\nu_r\Theta\\+f_f(1+\Theta-\nu_r\Theta-\nu_f-4\nu_r\nu_f\Theta)\end{bmatrix}E_rE_f(\mathbf{n})\end{aligned} \tag{20}$$

The case $\Theta = 1$ and $E_f(\mathbf{n}) = E_f$ corresponds obviously to the base model (9).

As a conclusion, note that in all cases (base model and three variations) the macroscopic behaviour of the composite remains transversely isotropic with axis **n** through the introduction of the Eshelby tensor of a cylindrical inclusion.

5. Reliability model and simulation procedure

As detailed above, the micromechanical scheme provides for each given morphology (components types and distribution) an estimation of the overall behaviour and average local fields (respectively from Eqs. (3) and (4)). In order to introduce uncertainties and establish their influence, this section aims at coupling such deterministic mechanical representation with reliability analysis. It should be noted that the relevance of the approach relies on the availability of statistical experimental characterizations, especially to define the distribution of random variables and failure scenario. Accordingly, the paper focuses on mechanical monotonic solicitations of the composite materials investigated by manufacturers; long-term durability effects (fatigue or extreme environmental conditions) are not considered here.

The development follows the three general steps described in the first section.

5.1. Random variables

Uncertainties sources retained in this paper concerns:

- on one hand, the materials data (resin, fibres and composite): components mechanical properties (elastic behaviour and yield strength), the microstructural phases distribution (fibres volume fraction) and the composite geometry (rods diameter),
- on the other hand, the micromechanical modelling: porosity of the matrix, fibres shape and behaviour.

Without any specific correlation characterization, all random variables are assumed to be independent. The estimation of the failure probability (1) can be done in that case only from the individual distribution functions f_{X_i} associated to each random variables X_i. Classically, microstructural reliability approaches favour the Weibull model to account for the distribution of random variables, especially for strength parameters. This choice, which is based on the weakest link assumption, allows to account for some scale effect [22]. In the present case, data relative to fibres and composite have been obtained on samples of same length, the scale effect can reasonably be neglected. Moreover, our interest is to deal as much as possible with available data, that are given here through mean values of parameters with possibly lower and upper bounds (Tables 1 and 2). It seems then more relevant to turn to the Normal distribution function which provides the ratios included within mean centred intervals.

Precisely, for random variables X_i associated to materials data, one retains the mean value $\overline{X_i}$ provided by manufacturers or literature (case of Poisson ratios) and the standard deviation S_{X_i} is taken such that 99.73% of the data values are included between given intervals (for the Normal distribution, $Prob(\overline{X} - 3S_X \le X \le \overline{X} + 3S_X) = 99.73\%$). As an example, one retains following distribution parameters for the resin Young modulus:

$$\overline{E_r} = 2800 \text{ MPa}, \quad S_{E_r} = \frac{125}{3} \simeq 42 \text{ MPa} \tag{21}$$

If the deviation interval is not specified, one considers that 99.73% of the data values are included within $[0.9\overline{X}, 1.1\overline{X}]$ by choosing

$$S_X = \frac{10\% \times \overline{X}}{3} \tag{22}$$

Since modelling uncertainties concern physical or mechanical features, we have chosen values consistent with their nature and with the bibliography [14,15]. For instance, the matrix porosity f_p and mechanical contrast Θ that are investigated in what follows are restricted to

$$\overline{f_p} \le 10\%, \quad 0.01 \le \Theta \le 0.07 \tag{23}$$

As before, the standard deviation is defined by Eq. (22).

5.2. Failure scenario

In this study, the reliability of the composite rod corresponds to its mechanical strength achievement under monotonic loads since failure data provided by manufacturers (TORAY and SOFICAR) deal only with such solicitations. Precisely, the composite failure point is defined as its yield strength which is governed by local damage behaviours. For fibre-reinforced materials, this may be related either to components failure (fibres and matrix) or interfaces microcracking. In the case of stay cables submitted to longitudinal tension, the predominant failure mode basically corresponds to the fibres breakage [14,15].

As said before, fibres are studied together, assuming identical geometry and mechanical behaviour (namely brittle elastic). From this, their failure point can be treated in a global manner with a limit state function of classical form:

$$G = \sigma_f^F(\mathbf{n}) - \langle \sigma_I \rangle_{(f)} \tag{24}$$

where $\langle \sigma_I \rangle_{(f)}$ denotes the maximum principal value of the average stress over the fibres phase given by the localization expression (4). The composite material is then considered as failed (not reliable) when the average mechanical state over fibres within the composite reaches the fibres axial failure strength. Contrary to existing works that restrict the probabilistic character to the strength [7–10], note that the present coupled approach accounts for the variability of both the strength (here $\sigma_f^F(\mathbf{n})$ described by Table 1) and the solicitation (here $\langle \sigma_I \rangle_{(f)}$ described by Tables 1 and 2 through Eq. (4)). Accordingly, the influence of uncertainties on both strength parameters and elastic properties is integrated and leads to a more complete representation and understanding of variability effects.

As a comment, the global representation of the fibres failure adopted through criterion (24) is clearly restricted to the present configuration (unidirectional carbon reinforcement, axial load) for which the composite exhibit brittle elastic behaviour. For other materials (glass fibres reinforcement for instance) or other kinds of solicitations, one should introduce the progressive aspect of damage by differentiating the fibres strength (for example through values given by a random Weibull distribution) and the load sharing to provide an enriched reliability representation.

5.3. Reliability calculations

The selection of a probabilistic code is essentially based on its application range, computational efficiency and various abilities such as the combination with other tools (see [23] for a review). The free and open probabilistic code FERUM [24] has been chosen for various reasons. The present analysis requires quite simple calculations due to mechanical behaviours considered (brittle elastic) and explicit expressions provided by the Mori–Tanaka scheme. Moreover, one needs to set up easily this direct coupling with the micromechanical model and to derive complete sensitivities analyses to fulfill the purpose in view. Accordingly, a direct

coupling between FERUM and the micromechanical model has been set up:

- FERUM generates realizations of the random variables vector X, evaluates function G and its derivative necessary for the determination of P_f and for the sensitivity analysis,
- the mechanical model provides for each vector X the expression of the local stress entering the failure criterion (24).

Among computational methods, note that various approximation schemes have been investigated and compared (see Table 3) and, accordingly, the approximation method FORM has been used in most cases since it requires less calls to the failure function G for equivalent estimation of the probability of failure.

6. Results and discussion

This part aims at comparing simulation results and experimental data. Precisely, we investigate the failure probability of carbon-epoxy rods submitted to longitudinal tension tests. The macroscopic stress on the material is thus

$$\Sigma = \Sigma_{nn}\mathbf{n}\otimes\mathbf{n} \quad \text{with } \Sigma_{nn} = \frac{4F}{\pi\phi^2} \tag{25}$$

with F the longitudinal force applied.

6.1. Base model

As a beginning, the reliability analysis has been performed using the base model. Table 4 summarizes the seven random variables retained and the parameters of their distribution. Note that only Poisson ratios data (for resin and fibres) come from the literature, all others have been provided by manufacturers.

Simulation results of the failure probability are presented in Fig. 6 and compared with raw experimental data provided by SOFICAR. The model clearly leads to a poor representation of the failure probability. For example for the force $F=86$ kN, simulation gives $P_f=5\%$ whereas raw data comes around $P_f=35\%$; the $\mathcal{R}^2$ coefficient of determination confirms in both cases the bad correlation with experimental data (Table 5).

Among various reasons that can lead to such deviation, we have studied first the influence of the device uncertainties.

Table 3
Computational methods comparison.

Method	Calls to G	P_f (base model, $F=84$ kN)
FORM	45	1.6042×10^{-2}
SORM (Tvedt)	53	1.6568×10^{-2}
SORM (Breitung)	53	1.6493×10^{-2}
SORM (Hohenbichler-Rackwitz)	53	1.6571×10^{-2}
Monte Carlo	1000	1.65×10^{-2}

Table 4
Failure analysis—random variables (base model).

Variables	Mean value	Standard deviation
Epoxy Young modulus, E_r (MPa)	2800	42
Epoxy Poisson ratio, ν_r	0.4	0.01
Fibres Young modulus, E_f (MPa)	230 000	7667
Fibres Poisson ratio, ν_f	0.3	0.01
Fibres yield stress, $\sigma_f^F(\mathbf{n})$ (MPa)	4870	162
Fibres volume fraction, f_f (%)	67	2
Rod diameter, ϕ (mm)	6	0.03

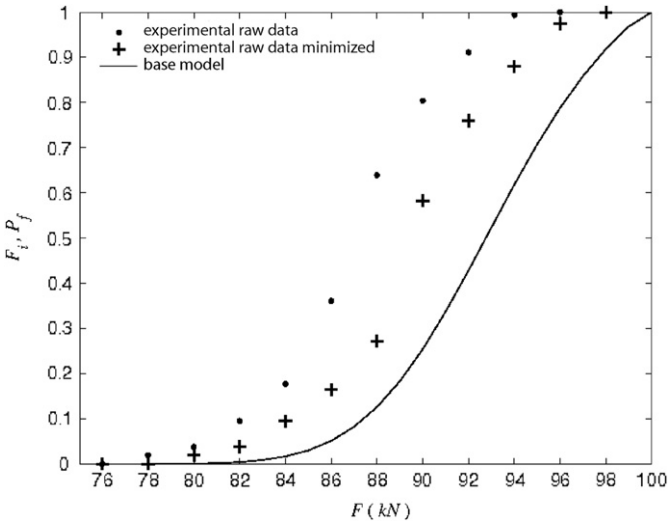

Fig. 6. Experimental cumulative frequencies F_i of the tensile strength $R^T(\mathbf{n})$ of carbon-epoxy rods and simulated failure probability P_f according to the load (base model).

Table 5
Coefficient of determination of the representations.

Experimental data	Raw data	3% minimized	Raw data	
Model	Base	Base	Corrected ($\overline{p_{act}}=95\%$)	
Range of comparison		$P_f\le1$		$P_f\le0.4$
$\mathcal{R}^2$	0.24	0.64	0.95	0.98

Table 6
Failure analysis—supplementary random variables.

Variables	Mean value	Standard deviation
Resin porosity, f_p (%)	10	0.3
Fibres aspect ratio, λ	0.5	0.02
Anisotropic contrast, Θ	0.05	0.002

Accordingly, simulated results have been compared with experimental raw minimized of 3% (maximum error provided by SOFICAR). If these variability tends to decrease the difference with the model (P_f ($F=86$ kN)$=18\%$, Fig. 6; important increase of $\mathcal{R}^2$, Table 5), the deviation remains yet too important to be explained only by such aspect.

As a consequence, we have considered in a second step the model uncertainties. The coupling with micromechanics makes such investigation possible. For this, in addition to variables used for the base model (Table 4), supplementary random variables have been introduced independently (respectively f_p, λ and Θ) to describe the uncertainties related respectively to the matrix porosity, fibres shape and fibres anisotropy (Table 6). For these three parameters, Fig. 7 shows that their influence on the failure probability of the composite rod is quite negligible compared to the base model, even for extreme values of some of them (for instance a porosity of 10% is not really acceptable for such products). In view of their respective impact, a simultaneous treatment of the three aspects would have led to the same conclusion. If such result is not surprising in the present context (in view of the composite and solicitation studied), the coupled approach makes it possible to confirm such expectations through probabilistic investigations. Accordingly, this analysis tends to justify the assumptions retained in the base formulation and to look after an other explanation of the deviation.

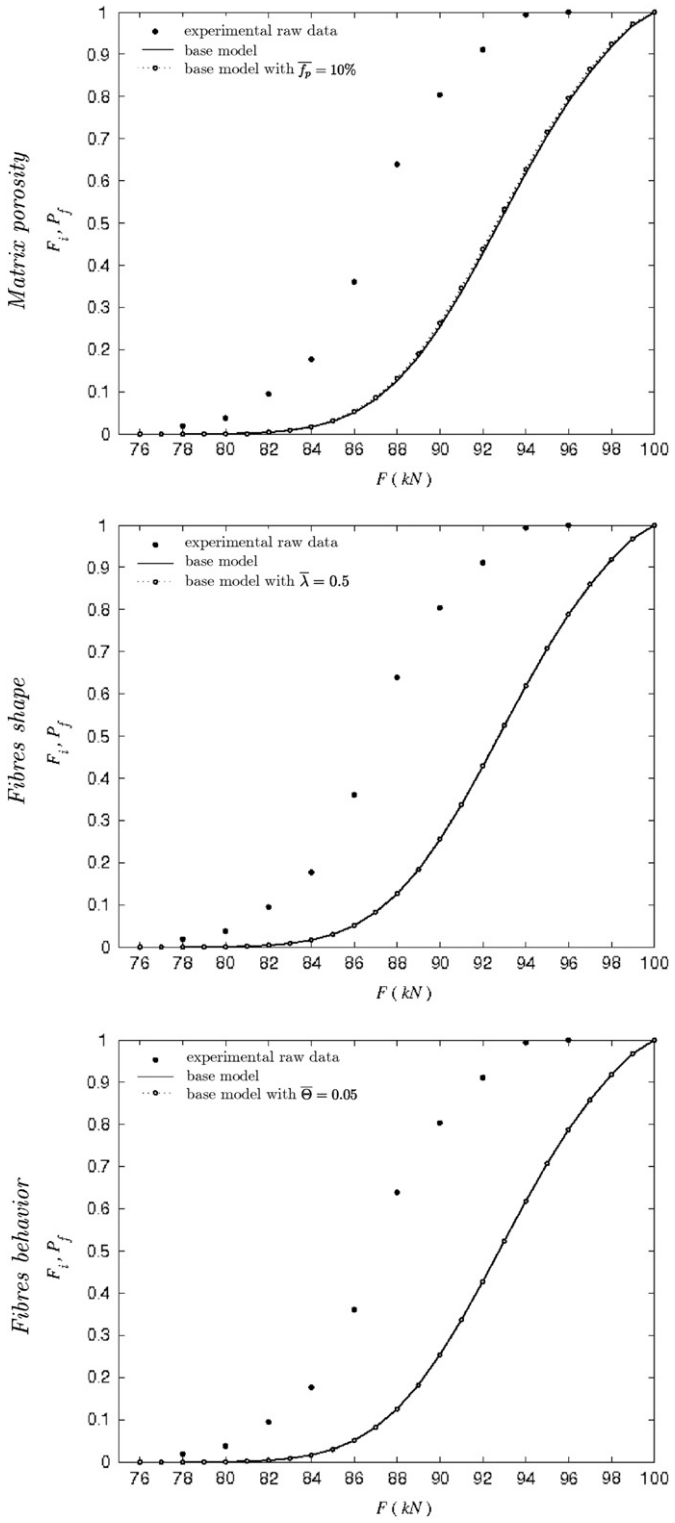

Fig. 7. Experimental cumulative frequencies F_i of the tensile strength $R^T(\mathbf{n})$ of carbon-epoxy rods and simulated failure probability P_f according to the load (base model with influence of the model uncertainties).

6.2. Model correction

In addition to the failure probability, a reliability analysis provides also interesting information that can help to clarify the problem. In particular, the sensitivities of P_f with respect to the variables mean values show that the fibres yield stress $\sigma_f^F(\mathbf{n})$ and the fibres volume fraction f_f play the most significant role on the rod reliability among microstructural parameters (Fig. 8). In order to separate the respective influence of these two features, we have chosen to study unidirectional carbon-epoxy composite laminates manufactured by SOFICAR (with high-strength carbon fibres T800H-2∗12K), and precisely their elastic behaviour for which the single impact of f_f can be analysed.

The Mori–Tanaka formulation gives rise to the following expression of the composite effective modulus $E(\mathbf{n})$ for the base model:

$$E(\mathbf{n}) = [\mathbf{n}\otimes\mathbf{n} : \mathbb{S}_{MT}^{hom} : \mathbf{n}\otimes\mathbf{n}]^{-1}$$
$$= D[(1-f_f)(1-v_f-2v_f^2)E_r + [1+v_r+f_f(1-v_r-2v_r^2)]E_f]^{-1} \quad (26)$$

with D given by (11). Introducing again a probabilistic model with the variabilities on microstructural parameters defined in Table 7, one can thus derive the theoretical distribution of such property by means of Monte Carlo simulations [25,26] and compare it to the experimental measures of the elastic modulus $E(\mathbf{n})$ realized by SOFICAR. Fig. 9 shows again a bad approximation of experimental results: the model leads indeed to an amount around 15% of plates such that $E(\mathbf{n}) \leq 178$ GPa whereas measures give at least 65%.

From this analysis, we can conclude that the deviation problem probably takes its origin in the definition of the fibres volume fraction f_f. In agreement with the expert evaluation of SOFICAR, it is indeed possible that all the fibres put in the composite may not be completely used due to various degradations during the manufacturing process (fibres cut or not perfectly impregnated) or to a bad position within the product (default in straightness). In order to translate such idea, we propose to introduce a new random parameter p_{act} characterizing the amount of fibres within the composite really active on the mechanical point of view.

In what follows, we propose then to deal with a corrected micromechanical model for which the fibres volume fraction used

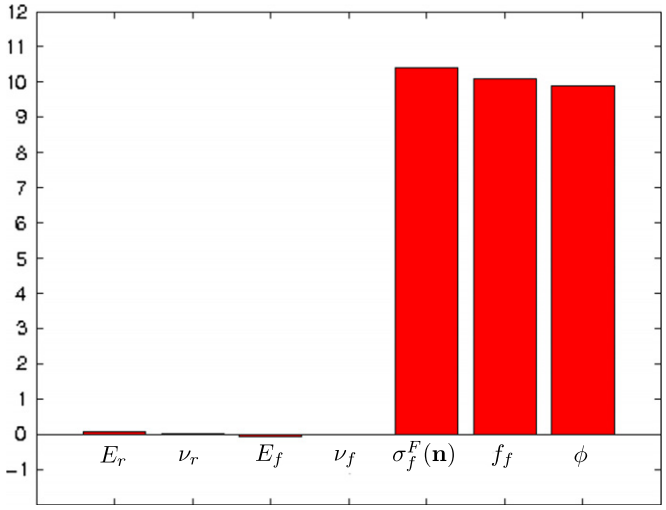

Fig. 8. Sensitivities with respect to the mean values of random variables (corrected model, $P_f = 10^{-2}$).

Table 7
Elastic modulus analysis—random variables (base model).

Variables	Mean value	Standard deviation
Epoxy Young modulus, E_r (MPa)	2800	42
Epoxy Poisson ratio, v_r	0.4	0.01
Fibres Young modulus, E_f (MPa)	294 710	7667
Fibres Poisson ratio, v_f	0.3	0.01
Fibres volume fraction, f_f (%)	67	2

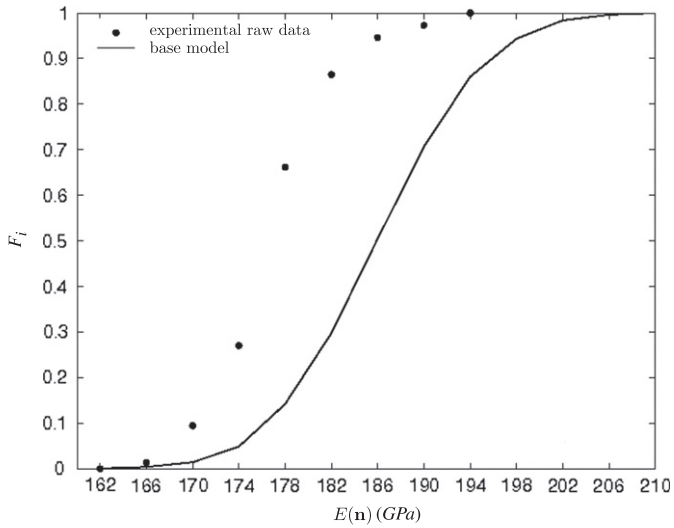

Fig. 9. Experimental cumulative frequencies F_i of the elastic modulus $E(\mathbf{n})$ of carbon-epoxy plates of rods and simulated theoretical distribution of $E(\mathbf{n})$ (base model).

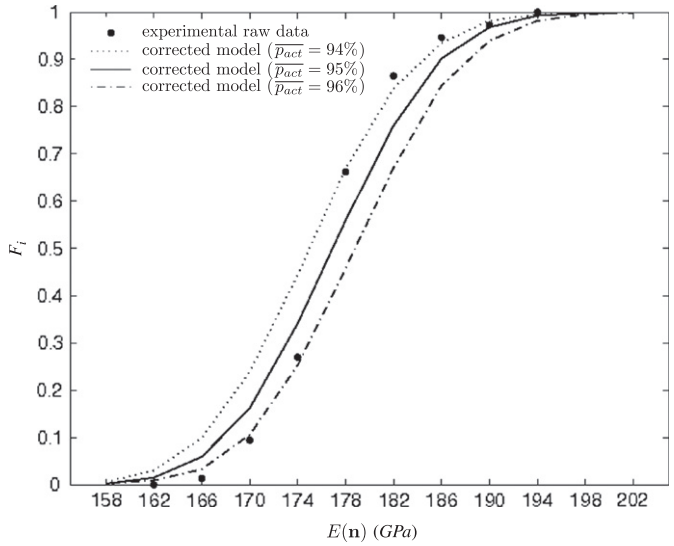

Fig. 10. Experimental cumulative frequencies F_i of the elastic modulus $E(\mathbf{n})$ of carbon-epoxy plates of rods and simulated theoretical distribution of $E(\mathbf{n})$ (corrected model).

in the Mori–Tanaka constitutive law is changed to:

$$f_f \rightarrow f'_f = p_{act} \times f_f \tag{27}$$

with $p_{act} \leq 100\%$. By definition, the identification of the distribution of the variable p_{act} requires microstructural observations of the manufactured composites. Since such information is not available in the present case, this variable is identified through the elastic response of composite plates. For this, the procedure consists in introducing in the probabilistic model the Normal random variable p_{act} with mean value $\overline{p_{act}}$ and standard deviation defined by Eq. (22) in addition to those described in Table 7, and in searching the value of $\overline{p_{act}}$ that leads to the best representation of the Young modulus $E(\mathbf{n})$. Fig. 10 shows that the best agreement with raw experimental data is obtained for a mean value $\overline{p_{act}} = 95\%$, which is rather a good ratio for the manufacturing process.

In order to estimate the influence of such correction of the mechanical model on the failure response of composite rods, we have introduce in the failure probabilistic model the Normal random variable p_{act} with identified mean value $\overline{p_{act}} = 95\%$ and standard deviation defined by Eq. (22) in addition to those already described in Table 4. Fig. 11 proves the clear improvement of the representation provided by the correction of the fibres volume fraction, which is confirmed also in Table 5 with even a coefficient of determination $\mathcal{R}^2 = 98\%$ for the range of $P_f \leq 0.4$. This constitutes a very satisfactory result in view of such complex and uncertain phenomena as composite failure.

Beyond the study of this quite simple application case, one of the main objectives of this part was to demonstrate here the enriched identification and validation phases allowed by such coupled micromechanical and reliability approach:

- for the checking of the mechanical model uncertainties since the influence of various features introduced within the formulation can be quantified,
- and, if required, for its correction by pointing out significant parameters and providing judicious guidelines to improve it.

The representative character of a micromechanical modelling is investigated in a more rational way, not limited to a comparison with some experimental tests but with an important number of results (here 74 measures for the identification of p_{act} and 158 measures for the validation of P_f). In the context of composite materials, this allows to integrate the inherent variability of their response, not to accept or reject a model on the base of a few results but, on the contrary, to provide an exhaustive and quantified analysis of its relevance towards an important number of experimental data.

6.3. Design optimization

We propose now to focus on another interest of the approach, useful this time for the development of composite materials. Once the model has been established and validated, it is indeed interesting to study the sensitivities of P_f that provides judicious guidelines for design optimization.

The sensitivities of P_f with respect to the variables mean values give first the most significant parameters for the structure reliability. For the corrected model, Fig. 12 shows that the mean values $\overline{\sigma_f^F(\mathbf{n})}$ of the fibres yield stress, $\overline{f_f}$ of the fibres volume

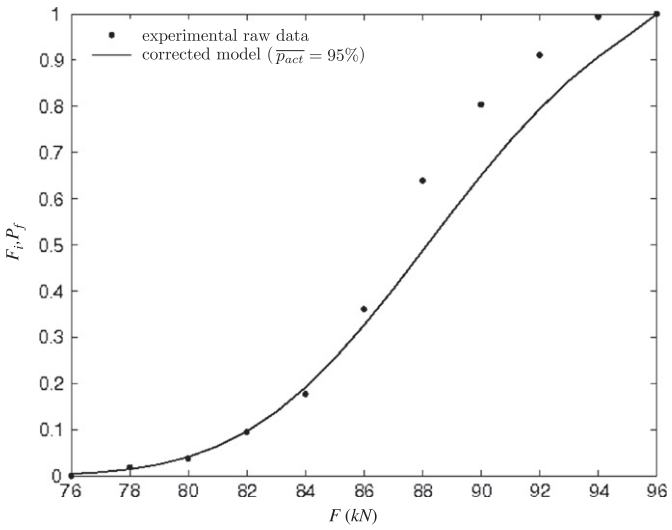

Fig. 11. Experimental cumulative frequencies F_i of the tensile strength $R^T(\mathbf{n})$ of carbon-epoxy rods and simulated failure probability P_f according to the load (corrected model).

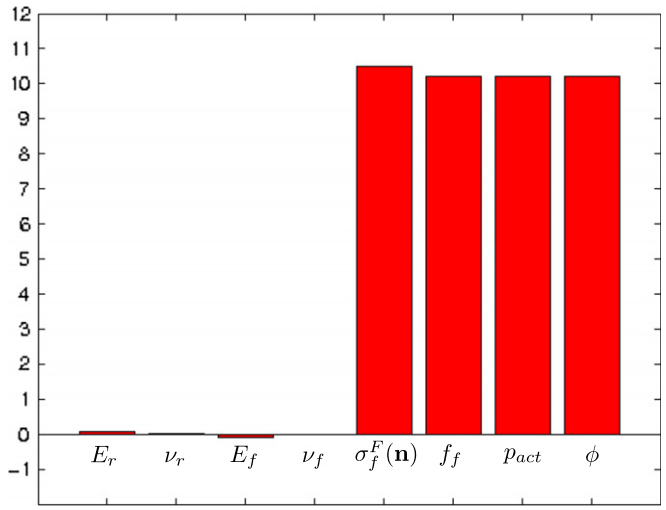

Fig. 12. Sensitivities with respect to the mean values of random variables (corrected model, $P_f=10^{-2}$).

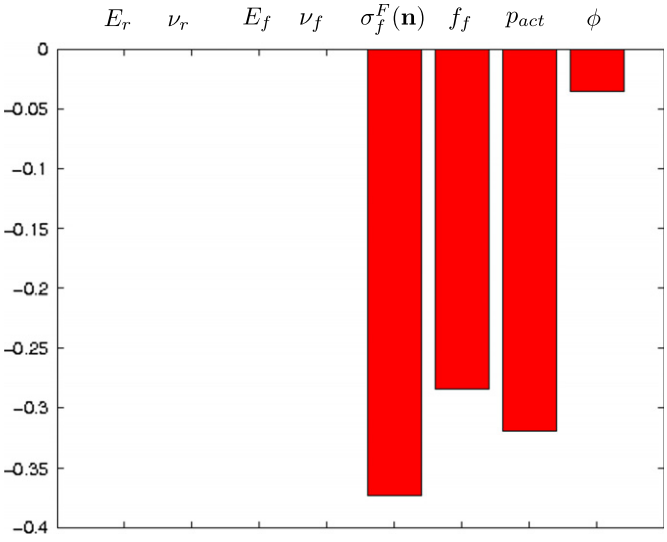

Fig. 13. Sensitivities with respect to the standard deviation of random variables (corrected model, $P_f=10^{-2}$).

fraction, $\overline{p_{act}}$ of the amount of active fibres and $\overline{\phi}$ of the rod diameter play the most important role. Precisely, this diagram indicates a similar positive impact of these variables on the reliability: a same increase in percent of each mean value will cause a same decrease of the failure probability. Accordingly, the coupled analysis allows to highlight the microstructural parameters that lead to the best improvements of the rod reliability, namely the kind of fibre for $\overline{\sigma_f^F(\mathbf{n})}$, the composite composition for $\overline{f_f}$ and the manufacturing process for $\overline{p_{act}}$, and to provide a quantitative estimation of their respective influence.

On the other hand, the study of the sensitivities of P_f with respect to the variables standard deviation helps for quality control with again a quantitative information. Fig. 13 shows the parameters whose deviation causes the most uncertainties in the composite response and then less reliability. Here, the coupled approach shows that a particular attention should be given to fibre manufacturing process (to ensure a reproductibility of the fibres yield stress $\sigma_f^F(\mathbf{n})$) and to the composite manufacturing process (to avoid strong deviations of the fibres volume fraction f_f and of the amount of active fibres p_{act}).

7. Conclusion and perspectives

Since microstructural parameters (constituents properties and their arrangement) and local failure phenomena have a significant impact on the macroscopic reliability of composite structures, the coupling between reliability analysis and micromechanics presented in this paper offers open perspectives for many aspects:

- for the progress of advanced material engineering, since it improves the understanding of uncertainties consequences, especially at the microscale;
- for the development, identification and validation of constitutive modelling, by providing a rational and enriched estimation of the relevance of micromechanical models;
- for the composites design and optimization, through a realistic and quantitative link between microstructural uncertainties and macroscopic performances (effective properties and failure response).

On the other hand, the implementation of such approach requires the availability of data relative both to micro- and macroscales, namely material physical characteristics and statistical responses, in order to justify, validate and, if necessary, calibrate the mechanical model.

Even if the application presented here has been handled on a quite simple case of composite material, failure mode and mechanical model, this allows however to explain and demonstrate clearly the capacities of the coupled approach. It can obviously be applied to more complex configurations, especially with micromechanical models that consider more microstructural features, interaction effects, plastic behaviours or progressive damage. The introduction within such approach of long-term effects (fatigue, durability), which particularly influence the composite reliability, should also be investigated to improve the representation.

Among perspectives to this work, it should be noted finally that such coupling can also be put in place up to a structure scale. Indeed, the probabilistic code FERUM allows also the coupling with finite-element softwares and the procedure can be applied to investigate the design of composite structures (see [27]).

Acknowledgements

Authors fully acknowledge the SOFICAR Company for technical data and support concerning composites materials and their manufacturing process. Special thanks also to Professor Karama of the National School of Engineers of Tarbes (ENIT) who made this work possible.

Appendix A

Let define the bases $\{\mathbb{F}_I\}_{I=1,6}$ and $\{\mathbb{G}_I\}_{I=1,12}$ of T^4 where the set $(\mathbf{n},\mathbf{t},\mathbf{k})$ represents an orthonormal basis of $\mathbb{R}^3$:

$$\begin{cases} \mathbb{F}_1 = \frac{1}{2}(\mathbf{I}-\mathbf{n}^{\otimes 2}) \otimes (\mathbf{I}-\mathbf{n}^{\otimes 2}) \\ \mathbb{F}_2 = \mathbf{n}^{\otimes 4} \\ \mathbb{F}_3 = (\mathbf{I}-\mathbf{n}^{\otimes 2})\overline{\otimes}(\mathbf{I}-\mathbf{n}^{\otimes 2}) - \frac{1}{2}(\mathbf{I}-\mathbf{n}^{\otimes 2}) \otimes (\mathbf{I}-\mathbf{n}^{\otimes 2}) \\ \mathbb{F}_4 = (\mathbf{I}-\mathbf{n}^{\otimes 2})\overline{\otimes}\mathbf{n}^{\otimes 2} + \mathbf{n}^{\otimes 2}\overline{\otimes}(\mathbf{I}-\mathbf{n}^{\otimes 2}) \\ \mathbb{F}_5 = \mathbf{n}^{\otimes 2} \otimes (\mathbf{I}-\mathbf{n}^{\otimes 2}) \\ \mathbb{F}_6 = (\mathbf{I}-\mathbf{n}^{\otimes 2}) \otimes \mathbf{n}^{\otimes 2} \end{cases} \tag{A.1}$$

$$\begin{cases} \mathbb{G}_1 = \mathbf{n}^{\otimes 4}, \quad \mathbb{G}_2 = \mathbf{t}^{\otimes 4}, \quad \mathbb{G}_3 = \mathbf{k}^{\otimes 4} \\ \mathbb{G}_4 = \mathbf{n}^{\otimes 2} \otimes \mathbf{t}^{\otimes 2}, \quad \mathbb{G}_5 = \mathbf{t}^{\otimes 2} \otimes \mathbf{n}^{\otimes 2} \\ \mathbb{G}_6 = \mathbf{t}^{\otimes 2} \otimes \mathbf{k}^{\otimes 2}, \quad \mathbb{G}_7 = \mathbf{k}^{\otimes 2} \otimes \mathbf{t}^{\otimes 2} \\ \mathbb{G}_8 = \mathbf{k}^{\otimes 2} \otimes \mathbf{n}^{\otimes 2}, \quad \mathbb{G}_9 = \mathbf{n}^{\otimes 2} \otimes \mathbf{k}^{\otimes 2} \\ \mathbb{G}_{10} = \mathbf{n}^{\otimes 2} \underline{\otimes} \mathbf{t}^{\otimes 2} + \mathbf{t}^{\otimes 2} \underline{\otimes} \mathbf{n}^{\otimes 2} \\ \mathbb{G}_{11} = \mathbf{t}^{\otimes 2} \underline{\otimes} \mathbf{k}^{\otimes 2} + \mathbf{k}^{\otimes 2} \underline{\otimes} \mathbf{t}^{\otimes 2} \\ \mathbb{G}_{12} = \mathbf{n}^{\otimes 2} \underline{\otimes} \mathbf{k}^{\otimes 2} + \mathbf{k}^{\otimes 2} \underline{\otimes} \mathbf{n}^{\otimes 2} \end{cases} \tag{A.2}$$

The Eshelby tensor of inclusions of various shape within an isotropic matrix (Young modulus E_m, Poisson ratio ν_m) is given by [17,18]

- for a spherical inclusion:

$$\mathbb{S}^E_{(m)} = \frac{2(4-5\nu_m)}{15(1-\nu_m)} \mathbf{I} \underline{\otimes} \mathbf{I} + \frac{5\nu_m - 1}{15(1-\nu_m)} \mathbf{I} \otimes \mathbf{I} \tag{A.3}$$

- for a cylindrical inclusion of axis $\mathbf{n}$ with circular section:

$$\mathbb{S}^E_{(m)} = \frac{1}{2(1-\nu_m)} \mathbb{F}_1 + \frac{3-4\nu_m}{4(1-\nu_m)} \mathbb{F}_2 + \frac{1}{2} \mathbb{F}_4 + \frac{\nu_m}{2(1-\nu_m)} \mathbb{F}_6 \tag{A.4}$$

- for a cylindrical inclusion of axis $\mathbf{n}$ with elliptical section of axes ($\mathbf{t}$,$\mathbf{k}$) and aspect ratio λ (Fig. 5):

$$\mathbb{S}^E_{(m)} = \sum_{l=1}^{12} g_l \mathbb{G}_l \tag{A.5}$$

with

$$\begin{cases} g_1 = 0, \quad g_2 = \dfrac{1}{2(1-\nu_m)} \left[\dfrac{1+2\lambda}{(1+\lambda)^2} + \dfrac{1-2\nu_m}{1+\lambda} \right], \\ g_3 = \dfrac{1}{2(1-\nu_m)} \left[\dfrac{\lambda^2+2\lambda}{(1+\lambda)^2} + (1-2\nu_m) \dfrac{\lambda}{1+\lambda} \right], \quad g_4 = 0, \\ g_5 = \dfrac{\nu_m}{1-\nu_m} \dfrac{1}{1+\lambda}, \quad g_6 = \dfrac{1}{2(1-\nu_m)} \left[\dfrac{1}{(1+\lambda)^2} - (1-2\nu_m) \dfrac{1}{1+\lambda} \right], \\ g_7 = \dfrac{1}{2(1-\nu_m)} \left[\dfrac{\lambda^2}{(1+\lambda)^2} - (1-2\nu_m) \dfrac{\lambda}{1+\lambda} \right], \quad g_8 = \dfrac{\nu_m}{1-\nu_m} \dfrac{\lambda}{1+\lambda}, \\ g_9 = 0, \quad g_{10} = \dfrac{1}{1+\lambda}, \\ g_{11} = \dfrac{1}{1-\nu_m} \left[\dfrac{1+\lambda^2}{2(1+\lambda)^2} + \dfrac{1-2\nu_m}{2} \right], \quad g_{12} = \dfrac{\lambda}{1+\lambda} \end{cases} \tag{A.6}$$

References

[1] Ditlevsen O, Madsen H. Structural reliability analyses. Chichester: Wiley & Sons; 1996.
[2] Lemaire M. Structural reliability. London: ISTE, Wiley & Sons; 2009.
[3] Markov KZ. Elementary micromechanics of heterogenous media. In: Markov KZ, Preziosi L, editors. Heterogenous media. Boston: Birkhäuser; 2000. p. 1–162.
[4] Zaoui A. Continuum micromechanics: survey. J Eng Mech 2002;128:808–16.
[5] Bornert M, Bretheau T, Gilormini P. Homogenization in mechanics of materials. London: ISTE, Wiley & Sons; 2009.
[6] Graham-Brady LL, Arwade SR, Corr DJ, Gutiérrez MA, Breysse D, Grigoriu M, et al. Probability and materials: from nano- to macro-scale—a summary. Prob Eng Mech 2006;21:193–9.
[7] Gao Z. Reliability of composite materials under general plane loadings. J Reinf Plastics Compos 1993;12:430–56.
[8] Baxevanakis C, Jeulin D, Lebon B, Renard J. Fracture statistics modeling of laminate composites. Int J Solids Struct 1998;35:2505–21.
[9] Desrumaux F, Meraghni G, Benzeggagh ML. Micromechanical modeling coupled to a reliability approach for damage evolution prediction in composite materials. Appl Compos Mater 2000;7:231–50.
[10] Calard V, Lamon J. Failure of fiber bundles. Compos Sci Technol 2004;64:701–10.
[11] Hohenbichler M, Rackwitz R. Sensitivities and importance measure in structural reliability. Civil Eng Syst 1986;3:203–9.
[12] Kamchandani A, Cornell CA. Sensitivity estimation within first and second order reliability methods. Struct Saf 1992;11:95–107.
[13] Geffroy RL. La passerelle de Laroin. Freyssinet Mag 2002;214.
[14] Berthelot J-M. Composite materials—mechanical behavior and structural analysis. New-York: Springer-Verlag; 1999.
[15] Miracle DB, Donaldson SL. ASM handbook—composites, vol. 21. ASM International; 2001.
[16] SOFICAR, Technical Reports of Experimental Characterizations on Pultruded Composites: Experimental Device, Testing Results; 2001.
[17] Gilormini P, Bréchet Y. Syntheses: mechanical properties of heterogeneous media: which material for which model? Which model for which material? Modelling Simulation Mater Sci Eng 1999;7:805–16.
[18] Mori T, Tanaka K. Average stress in matrix and average elastic energy of materials with misfitting inclusions. Acta Metall 1973;21:571–4.
[19] Benveniste Y. A new approach to the application of Mori–Tanaka's theory in composite materials. Mech Mater 1987;6:147–57.
[20] Mura T. Micromechanics of defects in solids. The Hague: Martinus Nijhoff; 1987.
[21] Nemat Nasser S, Hori M. Micromechanics: overall properties of heterogenous materials. Amsterdam: Elsevier; 1993.
[22] Sutherland LS, Shenoi RA, Lewis SM. Size and scale effects in composites: I. Literature review. Compos Sci Technol 1999;59:209–20.
[23] Pellissetti MF, Schuëller GI. On general purpose software in structural reliability—an overview. Struct Saf 2006;28:3–16.
[24] Haukaas L. FERUM User's Guide, University of California ⟨www.ce.berkeley.edu/FERUM/⟩, 2000.
[25] Mullen RL, Ballarini R, Yin Y, Heuer AH. Monte Carlo simulation of effective elastic constants of polycrystalline thin films. Acta Mater 1997;45:2247–55.
[26] Grigoriu M. Stochastic mechanics. Int J Solids Struct 2000;37:197–214.
[27] Dehmous H, Welemane H. Multi-scale reliability analysis of composite structures—application to the Laroin footbridge. Eng Failure Anal 2010;18:988–98.